Am J Physiol Cell Physiol. Author manuscript; available in PMC 2011 November 30.

Published in final edited form as:
Am J Physiol Cell Physiol. 2010 June ; 298(6): C1376–C1387. doi:10.1152/ajpcell.00408.2009.

Extracellular signal regulated kinase and GEF-H1 mediate depolarization-induced Rho activation and paracellular permeability increase

Faiza Waheed, **Pam Speight**, **Glenn Kawai**, **Qinghong Dan**, **András Kapus**, and **Katalin Szászi**

Keenan Research Centre in the Li Ka Shing Knowledge Institute, St. Michael's Hospital and Dept. of Surgery, University of Toronto, ON, Canada

Abstract

Plasma membrane depolarization activates the Rho/Rho kinase (ROK) pathway and thereby enhances myosin light chain (MLC) phosphorylation, which in turn is thought to be a key regulator of paracellular permeability. However, the upstream mechanisms that couple depolarization to Rho activation and permeability changes are unknown. Here we show that three different depolarizing stimuli (high extracellular [K^+], the lipophilic cation tetraphenylphosphonium or L-alanine, which is taken up by electrogenic Na^+-cotransport) all provoke robust phosphorylation of Extracellular Signal Regulated Kinase (ERK) in LLC-PK1 and MDCK cells. Importantly, inhibition of ERK prevented the depolarization-induced activation of Rho. Searching for the underlying mechanism, we have identified GEF-H1 as the ERK-regulated critical exchange factor, responsible for the depolarization-induced Rho activation. This conclusion is based on our findings that a) depolarization activated GEF-H1, but not p115RhoGEF; b) siRNA-mediated GEF-H1 silencing eliminated the activation of the Rho pathway; c) ERK inhibition prevented the activation of GEF-H1. Moreover, we found that the Na^+/K^+ pump inhibitor ouabain also caused ERK, GEF-H1 and Rho activation, partially due to its depolarizing effect. Regarding functional consequences of this newly identified pathway, we found that depolarization increased paracellular permeability in LLC-PK1 and MDCK cells, and this effect was mitigated by inhibiting myosin using blebbistatin or a dominant negative (phosphorylation-incompetent) MLC. Taken together, we propose, that the ERK/GEF-H1/Rho/ROK/pMLC pathway could be a central mechanism whereby electrogenic transmembrane transport processes control myosin phosphorylation and regulate paracellular transport in the tubular epithelium.

Keywords

membrane potential; Rho family small GTPases; phospho-myosin; tubular epithelium; Rho exchange factors

Please address correspondence to: Katalin Szaszi, St. Michael's Hospital, Queen Wing 7-009, 30 Bond Street, Toronto, ON, Canada, M5B 1W8. Tel: 1 416 864 6060 ext 2838. Fax: 1 416 864 5167. szaszik@smh.toronto.on.ca.

INTRODUCTION

The resting plasma membrane potential contributes to the maintenance of cellular ionic homeostasis and provides driving force for electrogenic ion transport. In excitable cells, such as neurons and muscle cells, normal function is associated with large fluctuations of the membrane potential mediated by a variety of ion channels. In non-excitable cells, where the resting potential is relatively stable, physiological alterations in the potential can result from various electrogenic ion transport processes, such as activation of the Na^+-coupled amino acid and glucose cotransporters (31) or stretch-induced channels (55). In addition, pathological conditions, such as ATP depletion during hypoxia or metabolic substrate deprivation, and oxidative stress can also perturb the normal membrane potential (5, 10, 26). Thus, while physiological potential changes signify an altered functional state of the cells, a large and sustained depolarization can be associated with injury. In all of these cases adequate adaptive and protective cellular responses are needed. Therefore, it is not surprising that depolarization, similar to other physical factors, including aniso-osmolarity (39) or heat shock (3), was shown to activate various cellular signaling pathways.

Signals initiated by depolarization have been first described in neurons and neuron-like cells (21, 22). In the past years however, we (57) and others (12–14) have shown that depolarization-induced morphological changes occur in epithelia as well. For example, in cultured eye epithelial cells depolarization causes reorganization of F-actin and microtubules and the appearance of intercellular gaps (12, 14). Chifflet et al demonstrated that wounding of an epithelial monolayer results in depolarization of the plasma membrane in the cells bordering the wound. The ensuing actin rearrangement likely contributes to wound healing (13). Our own studies have demonstrated that in LLC-PK1 and MDCK kidney tubular cells depolarization elevates phosphorylation of the myosin light chain (MLC) (57). Interestingly, in contrast to neurons, where the depolarization-induced changes are mostly due to influx of Ca^{2+} through voltage-sensitive channels (e.g. (21)), MLC phosphorylation in the tubular cells is independent of intracellular Ca^{2+}. This observation pointed to a mechanism distinct from the classical Ca^{2+}-myosin light chain kinase (MLCK) pathway. In search of this mechanism, we found that depolarization activates RhoA, a major cytoskeleton-regulating small GTPase, and the ensuing Rho kinase (ROK) activation results in enhanced MLC phosphorylation (57). Two main questions, however, remained unanswered: the upstream mechanism of Rho activation and the possible effects of depolarization on epithelial transport processes.

With regards to signaling upstream of Rho in tubular epithelium, we have recently shown that the Extracellular Signal Regulated Kinase (ERK) mediates Tumor Necrosis Factor-α (TNF-α)-induced Rho activation (34). Importantly, multiple studies have demonstrated that in neurons and PC12 pheochromocytoma cells depolarization activates ERK (e.g. (4, 46, 48)). This prompted us to ask whether depolarization could activate ERK in epithelial cells as well, and if so, whether ERK could mediate depolarization-induced Rho activation.

Activation of small GTPases is promoted by GTP/GDP exchange factors (GEFs), which constitutes a large family (50). Rho GEF(s) regulated by depolarization have not yet been identified. GEF-H1, a microtubule and junction-bound Rho GEF ((6, 40) and reviewed in

(7)) is a good candidate since a) it is expressed in tubular cells, b) it has been implicated in paracellular permeability control in tubular cells (6, 34) and c) it was shown to be regulated by ERK (23). Interestingly, GEF-H1 was recently also found in complex with the AMPA receptor in neurons, which mediates fast synaptic potential changes (35). In light of these data, we aimed to examine the possible role of GEF-H1 in mediating depolarization-induced effects.

We also wished to investigate the functional consequences of the depolarization-induced myosin phosphorylation in tubular cells. The phosphorylation state of MLC is a key determinant of transepithelial and paracellular transport processes (32, 36, 54, 60). Since our previous studies have shown that depolarization, triggered by the electrogenic Na^+-alanine transporter, also induces myosin phosphorylation (57), it was conceivable that depolarization could serve as a coupling signal between electrogenic cotransporters and the paracellular pathway (36). The possible effects of depolarization on the intercellular junctions and paracellular pathway however remained to be established.

Based on this scenario, the aim of the current study was to investigate the mechanisms underlying depolarization-induced Rho activation. We wished to explore a possible role for the ERK pathway and GEF-H1. We also sought to investigate whether depolarization affects paracellular permeability, and whether this effect requires myosin phosphorylation. Here we show that depolarization activates ERK in tubular epithelial cells, and the ERK pathway mediates Rho activation. We have identified GEF-H1 as the exchange factor required for depolarization-induced, ERK-mediated Rho activation. Finally, we found that depolarization elevates paracellular permeability through phospho-MLC.

MATERIALS AND METHODS

Materials and antibodies

PD98059, U0126 and PP2 were from EMD Biosciences (Mississauga, On). BAPTA-AM was from Invitrogen (Burlington, On). L-alanine, tetraphenylphosphonium chloride (TPP^+), valinomycin, ouabain octahydrate, Epidermal Growth Factor (EGF), (−)-Blebbistatin and ionomycin (Iono) were from Sigma Aldrich Chemical Co. (St Louis, MO). Bovine serum albumin (BSA) was from BioShop Canada (Burlington, On). Complete Mini Protease inhibitor tablet and PhosSTOP Phosphatase Inhibitor tablet were from Roche Diagnostics (Laval, QC) and the BaculoGold protease inhibitor cocktail was from BD Pharmingen (Mississauga, ON).

Antibodies against the following proteins were used: RhoA, phospho-p44/42 MAPK (ERK1/2) (Thr202/Tyr204), ERK1 (used for immunostaining), phospho-MEK1/2 (Ser217/221), total MEK1/2, GEF-H1, p115RhoGEF, di-phosphorylated (Thr18, Ser19,) MLC and total MLC from Cell Signaling Technology (Danvers, MA); ERK1/2 (used for Western blotting) and myc from Santa Cruz Biotechnology Inc (Santa Cruz, CA); GAPDH from EMD Biosciences; Ras from Thermo Fisher Scientific (Nepean, ON) and Histone (H1 + core proteins) from Millipore (Billerica, MA). Peroxidase and Cy3-labelled secondary antibodies were from Jackson ImmunoResearch (West Grove, PA). Protein A/G agarose was

from Santa Cruz Biotechnology Inc. and the glutathione-Sepharose beads from GE Healthcare Lifesciences (Piscataway, NJ). DAPI nucleic acid stain was from Invitrogen.

Cells

LLC-PK_1, a kidney proximal tubule epithelial cell line, and MDCKII, a canine distal tubular epithelial cell line were obtained from the American Type Culture Collection. Both cell lines were maintained in DMEM medium supplemented with 10% fetal bovine serum and 1% antibiotic suspension (Penicillin and Streptomycin, Invitrogen) in an atmosphere containing 5% CO_2.

Media and cell treatment

The sodium-based medium (referred to as Na^+-medium) consisted of 130 mM NaCl, 3 mM KCl, 1 mM $MgCl_2$, 1 mM $CaCl_2$, 5 mM glucose, and 20 mM Na-Hepes (pH 7.4). The potassium-based medium (referred to as K^+-medium) contained 130 mM KCl, 1 mM $MgCl_2$, 1 mM $CaCl_2$ and 20 mM Hepes, pH 7.4. Confluent cells were serum-depleted for 3 h in DMEM prior to the experiments, followed by 15 min incubation in Na^+-medium prior to the indicated treatments.

Vectors and transient transfection

The vectors used were kind gifts from the following investigators: cDNAs encoding for the GST-RBD portion of Rhotekin and GST-RhoG17A (24) were from Dr. K. Burridge (University of North Carolina, Chapel Hill); AA-MLC vector (16) from Dr. H. Hosoya (Dept. Biological Sciences, Hiroshima University). GFP-tagged DN-K-Ras was described in (68). LLC-PK_1 cells were transfected using the transfection reagent FuGENE 6 (Roche Molecular Biochemicals) according to the manufacturer's instructions using 1 μg DNA/well for 6-well plates.

Short interfering RNA

The siRNA targeting the sequence in porcine GEF-H1 AACAAGAGCATCACAGCCAAG (obtained from Applied Biosytems/Ambion Inc (Austin, TX)) was described earlier (34). Cells were transfected with 100 nM siRNA oligonucleotide using the Lipofectamine™ RNAiMAX Transfection Reagent (Invitrogen) according to the manufacturer's instructions. Control cells were transfected with 100 nM Silencer siRNA negative control # 2 (non-related siRNA) (Applied Biosytems/Ambion). Experiments were performed 48 hours after transfection. The levels of GEF-H1 were routinely checked by Western blotting.

Generation of a polyclonal stable AA-MLC cell line

Generation of the AA-MLC expressing cell line was previously described (34). Briefly, retroviral vectors expressing a non-phosphorylatable, dominant negative version of MLC (in which T18 and S19 were replaced with alanines: AA-MLC) was used to transduce LLC-PK_1 cells. Control cells were transduced using the empty vector lacking the AA-MLC insert but harboring G418 resistance. Cells were selected using 1 mg/ml G418 starting at 48 h after transfection. AA-MLC expression was routinely checked by immunofluorescence using an anti-myc antibody and was ≥80%.

Western Blotting

Following treatment, cells were lysed on ice with cold lysis buffer (100 mM NaCl, 30 mM Hepes (pH 7.5), 20 mM NaF, 1 mM EGTA, 1% Triton X-100, supplemented with 1 mM Na_3VO_4, 1 mM PMSF, and protease inhibitors). For the detection of phospho-proteins the lysis buffer was also supplemented with the PhosSTOP phosphatase inhibitor. SDS-PAGE and Western blotting was performed as in (34). Blots were blocked in Tris-buffered saline containing either 5% BSA or 5% milk, and incubated with the primary antibody overnight. Antibody binding was visualized with the corresponding peroxidase-conjugated secondary antibodies and the enhanced chemiluminescence method (kit from GE Healthcare Lifesciences). Where indicated, blots were stripped and reprobed to demonstrate equal loading or detect levels of GEF-H1. As the phospho-ERK (pERK) antibody proved difficult to strip, these blots were first developed using total ERK antibody, followed by reprobing with pERK. Alternatively, in some cases the samples were run in duplicate and one blot was developed for ERK, the other for pERK.

Detection of myosin phosphorylation by urea-glycerol PAGE

Non-, mono-, and di-phosphorylated forms of MLC were separated using non-denaturating urea-glycerol polyacrylamide gel electrophoresis (PAGE) as described in our previous studies (57), with minor modifications. Briefly, confluent LLC-PK1 cells grown in six-well plates were serum depleted for 3 h and treated as indicated in the figure legends. Subsequently, the cells were lysed in ice-cold acetone containing 10% TCA and 10 mM DTT, followed by centrifugation for 5 min at 6000 rpm (4°C). The resulting pellet was washed with pure acetone, allowed to air dry, and dissolved in 50 μl of sample buffer containing 8.02 M urea, 234 mM sucrose, 23 mM glycine, 10.4 mM DTT, 20 mM Tris (pH 8.6), and 0.01% bromophenol blue. Samples were separated on a 12% urea-glycerol gel and blotted onto nitrocellulose membrane. Myosin light chain was detected by Western blotting using an anti-MLC antibody. Total MLC (i.e., the sum of all 6 bands) was determined by performing densitometry in each lane, and the amount of di-phosphorylated MLC was expressed as a percentage of total MLC in the same lane. This normalization allows direct comparison among the samples and prevents any potential errors that might arise from differences in loading. The blots were stripped and reprobed with an antibody against di-phospho-MLC.

Preparation of nuclear Extracts

Nuclear extracts were prepared from confluent layers of LLC-PK1 cells grown on 6-cm dishes, as in (43), using the NE-PER Nuclear Extraction Kit from Pierce Biotechnology (Rockford, IL) according to the manufacturer’s recommendation. The nuclear extracts were collected and their protein concentration determined. Samples containing 10 μg protein were analyzed by Western blotting. Anti-histone antibody was used to check for equal loading of nuclear proteins.

Preparation of Glutathione-Transferase-Rho-Binding Domain (GST-RBD) and GST-RhoG17A Fusion Proteins

GST-RBD (RhoA-binding domain (RBD): amino acids 7-89 of Rhotekin) and GST-RhoG17A beads were prepared as described (17, 34). Protein bound to the beads was estimated by SDS-PAGE, followed by Coomassie Blue staining, and the beads were kept at 4 °C for immediate use, or stored frozen in the presence of glycerol.

Rho activity assay

The amount of active RhoA was determined using an affinity precipitation assay with GST-RBD as in our earlier studies(34). Briefly, confluent LLC-PK_1 cells grown on 6 or 10-cm dishes were treated as indicated in the respective Figure legends. Cells were lysed with ice-cold lysis buffer containing 100 mM NaCl, 50 mM Tris base (pH 7.6), 20 mM NaF, 10 mM $MgCl_2$, 1% Triton X-100, 0.5% deoxycholic acid, 0.1% SDS, 1 mM Na_3VO_4 and protease inhibitors. After centrifugation, aliquots for determination of total RhoA were removed. The remaining supernatants were incubated at 4 °C for 45 min with 20–25 μg of GST-RBD beads, followed by extensive washing. Total cell lysates and the RBD-captured proteins were analyzed by Western blotting using RhoA antibody. Results were quantified by densitometry, and the amount of active RhoA in each sample was normalized to the corresponding total RhoA. The data obtained in each experiment were expressed as fold increase compared to the level of the control taken as unity.

Affinity precipitation of activated GEFs

For detection of activated GEF-H1, active GEFs were affinity precipitated from cell lysates using the RhoG17A mutant that cannot bind nucleotide and therefore has high affinity for GEFs (24) as in our earlier work (34). GEF-H1 or p115RhoGEF in the precipitates were detected by Western blotting. Precipitation with glutathione-Sepharose beads, containing no fusion proteins resulted in no GEF-H1 or p115RhoGEF precipitation (34). The GEFs in total cell lysates were also detected for each sample (total GEF-H1 or p115). Precipitated (active) and total GEF-H1 was quantified by densitometry. The amount of active GEF-H1 in each sample was normalized to the corresponding total GEF-H1 and the data obtained in each experiment were expressed as fold increase compared to the control taken as unity.

Ras activity assay

The amount of active Ras was determined using affinity precipitation with the Ras binding domain of the c-Raf kinase coupled to agarose beads (Cytoskeleton Inc). The precipitation assay was performed essentially as the Rho activation assay, using a lysis buffer that contained 150 mM NaCl, 25 mM Hepes (pH 7.5), 10 mM $MgCl_2$, 1 mM EDTA, 1% Ipegal CA-630, 10% glycerol, supplemented with 1 mM Na_3VO_4 and protease inhibitors. Total cell lysates and the pelleted beads were analyzed by Western blotting using a Ras antibody and quantified as described for Rho.

Immunofluorescence microscopy

Confluent cells grown on coverslips were treated as indicated in the corresponding Figure legends and fixed with 4% paraformaldehyde. Immunofluorescent staining was carried out

as in (34). Briefly, following permeabilization with Triton X-100, the coverslips were blocked with 3% BSA in phosphate buffered saline, followed by incubation with primary antibody (1:100). Bound antibody was detected using the corresponding fluorescent secondary antibody (1:1000), which also contained Dapi to counterstain nuclei. Cells were viewed using an Olympus IX81 microscope (Melville, NY) coupled to an Evolution QEi Monochrome camera (Media Cybernetics, Bethesda, MD).

Transepithelial permeability measurements

Control or AA-MLC expressing LLC-PK_1 or MDCK cells were grown on Transwell filters (Costar, pore size 0.4 μm) for 1 day after becoming confluent. The medium in both the top and bottom compartments was replaced with Na^+- medium for 15 minutes. To treat cells with the K^+-medium, the medium in both the top and the bottom was replaced. At the same time, the cells were exposed to 2 mg/ml FITC-labelled dextran (4 kDa, Sigma Aldrich Chemical Co) added to the top compartment. After 3 h, 50 μl samples were taken from the bottom compartment, and the fluorescence was determined by a fluorescent microplate reader (Fluoroscan Ascent FL) using 480 and 518 nm as the excitation and emission wavelength, respectively. We have previously shown that under these conditions LLC-PK1 cells form a size selective barrier, and remain impermeable to a 70 kDa FITC-labelled dextran (Sigma Aldrich Chemical Co) (34). The transport of the large molecular weight dextran was unchanged by treatment with K^+- medium (not shown).

Protein assay

Protein concentration was determined by the bicinchoninic acid assay (Pierce Biotechnology) or the Precision Red Advanced Protein Assay (Cytoskeleton Inc) with BSA used as standard.

Densitometry

Films with non-saturated exposures were scanned and densitometry analysis performed using a GS-800 calibrated densitometer and the “band analysis” option of the Quantity One software (BioRad). For analyzing ERK phosphorylation, in each experiment the densitometric data were expressed as the percent of the maximal effect. This representation allowed us to compare ERK phosphorylation even in experiments where the basal ERK phosphorylation was small and close to the background.

Statistical analysis

All shown blots and immunofluorescent pictures are representatives of at least three similar experiments. Data are presented as mean ± S.E. of the number of experiments indicated (n). Statistical significance was assessed by one-way ANOVA using the GraphPad Prism software.

RESULTS

Depolarization induces ERK phosphorylation in tubular cells

To investigate the role of the ERK pathway in mediating the depolarization-induced cytoskeleton remodeling and Rho activation, we first asked whether depolarization can induce ERK activation in tubular cells. Similar to our earlier study (57) we used a high [K^+] containing medium (K^+-medium) to induce depolarization in LLC-PK_1 and MDCK cells. As shown in Fig 1A, exposure of the cells to the K^+-medium resulted in a rapid increase in the amount of pERK in both cell types. In LLC-PK1 cells ERK phosphorylation was well detectable at 2 minutes, reached a maximum around 10 minutes and remained high at later times. This kinetics was very similar to the depolarization-induced myosin phosphorylation shown in our earlier work (57). K^+-medium also enhanced ERK phosphorylation in MDCK cells, showing that the effect is a general phenomenon and is not restricted to the proximal tubular cell line (Fig 1A, right blot). The effect of the K^+-medium on ERK phosphorylation proved to be reversible, as the readdition of Na^+-medium following treatment with elevated K^+ gradually reduced ERK phosphorylation to near basal levels within 10 minutes (Fig 1B). Next, to further substantiate that depolarization and not elevated K^+ concentration per se causes ERK phosphorylation, we induced depolarization using two alternative methods (57). We have previously shown that addition of the lipophilic cation, tetraphenyl phosphonium (TPP^+) to tubular cells causes rapid depolarization (57). Fig 1C shows that TPP^+ induces a fast and sustained elevation of pERK. We also tested the effect of L-alanine, which enters the cells through a Na^+-cotransport process and causes depolarization (31, 57). Challenging cells with 20 mM L-alanine resulted in a rapid increase in ERK phosphorylation (Fig 1D). This effect, however, followed different kinetics: after a fast peak, ERK phosphorylation dropped, but still remained above the basal level. Importantly, both TPP^+ and alanine caused enhanced ERK phosphorylation under conditions where the extracellular K^+ concentration remained constant and low. In summary, three different depolarizing stimuli induce ERK activation in tubular cells.

Next we performed immunostaining to localize pERK. In resting cells pERK was barely detectable (Fig 1E top left picture), which correlates well with the low pERK levels detected by Western blotting. In contrast, K^+-medium induced a marked increase in pERK both in the cytosol and in the nucleus (Fig 1E top right picture). Western blotting of total cell lysates and nuclear fractions showed that ERK was present in the nucleus of resting cells. While total ERK levels did not seem to significantly change in the nucleus upon K^+ treatment, pERK levels gradually increased, in parallel with the cytosolic pERK signal (Fig 1F). Thus, depolarization provokes a rise in pERK both in the cytosol and in the nucleus.

Depolarization-induced ERK activation is Ca^{2+}-independent and Ras dependent

Depolarization-induced ERK activation was previously shown in various neuronal cells (e.g. (4, 21, 46)). In these cells Ras and ERK activation was dependent on Ca^{2+} and calmodulin. Interestingly, we previously found that depolarization does not induce an increase in the intracellular Ca^{2+} levels in tubular cells (57). This suggests a different mechanism of ERK activation. To verify this, we examined the role of intracellular Ca^{2+} in the depolarization-induced ERK activation. LLC-PK1 cells were loaded with the calcium chelator BAPTA-AM

(30 μM), prior to exposure to K^+-medium, to prevent any increase in intracellular Ca^{2+} levels. As shown in Fig 2A ERK phosphorylation induced by the Ca^{2+} ionophore ionomycin was prevented, showing that BAPTA indeed eliminated increase in intracellular Ca^{2+} (Fig 2A right panel). In contrast, K^+-medium caused a similar elevation in ERK phosphorylation in control and BAPTA-loaded cells, suggesting that a rise in intracellular Ca^{2+} is not required for the effect.

Receptor-induced ERK activation is downstream of the Ras/Raf/MEK pathway (49). However, stretch-induced ERK activation was suggested to be independent of Ras (20). Therefore we next examined whether depolarization activates Ras in tubular cells. Ras activation was measured using an affinity precipitation assay with the GST-Ras Binding Domain of c-Raf. As demonstrated in Fig 2B, depolarization caused a rapid, ≈5-fold increase in the level of active Ras. Moreover, phosphorylation of MEK1/2 was also well detectable in the total cell lysates of the same samples (Fig 2B). To examine whether Ras is indeed necessary for the depolarization-induced ERK activation, we transfected LLC-PK1 cells with a GFP-tagged dominant negative (DN)-K-Ras and investigated the depolarization-induced ERK phosphorylation by immunofluorescence (Fig 2C). While the increase in ERK phosphorylation was readily detectable in the non-transfected cells exposed to high K^+-medium, the presence of DN-Ras eliminated this effect. Additional experiments verified that expression of the dominant negative Ras did not affect the level of total ERK (Fig 2D). Taken together, these data show that in tubular cells the Ras/Raf/MEK pathway mediates the effect of depolarization, independent of intracellular Ca^{2+}.

Depolarization-induced Rho activation is mediated by ERK

We have previously shown that depolarization induces activation of Rho, leading to Rho kinase-dependent MLC phosphorylation (57). We also found that in tubular cells Rho activation induced by TNF-α is ERK-dependent (34). Having established that depolarization induces ERK activation in tubular cells, with kinetics similar to Rho activation, we next asked whether ERK can mediate the depolarization-induced Rho activation. Consistent with our previous findings, K^+-induced depolarization caused a ≈3.5–7-fold increase in Rho activity (Fig 3A and B), as measured using the precipitation assay with the Rho binding domain of Rhotekin. Importantly, the depolarization-induced Rho activation was strongly inhibited in the presence of two different MEK1/2 inhibitors, PD98059 (Fig 3A) and U0126 (Fig 3B), which are known to prevent ERK activation. These data therefore suggest that the depolarization-elicited activation of Rho is mediated by the MEK/ERK pathway.

Depolarization activates the Rho exchange factor GEF-H1 in an ERK-dependent manner

The exchange factor mediating depolarization-induced Rho activation has not been identified. GEF-H1 is a key epithelial Rho exchange factor that is regulated by ERK (23, 34). To explore a potential role of this GEF in the depolarization-induced effects, we first followed changes in its activity. Cells were exposed to K^+-medium, and active GEFs were precipitated using a Rho mutant (GST-RhoG17A) that exhibits high affinity for activated GEFs (34). The presence of precipitated GEF-H1 was detected by Western blot analysis. As shown in Fig 3C, depolarization induced a more than 10-fold activation of GEF-H1.

Importantly, this depolarization-induced GEF-H1 activation was prevented by the MEK1/2 inhibitor PD98059 (Fig 3C).

To test whether the effect of depolarization on GEF-H1 is specific to this protein, we tested another Rho exchange factor, p115RhoGEF (1). As shown on Fig 3D, p115RhoGEF was precipitated using RhoG17A under basal conditions, suggesting that it is active in resting cells. However, in contrast to GEF-H1, the amount of active p115 did not increase when cells were stimulated by the K^+-medium.

GEF-H1 mediates the depolarization-induced activation of the Rho pathway

Having shown that GEF-H1 is activated by depolarization, we next assessed whether it indeed mediates Rho activation. We used a GEF-H1 specific siRNA, that efficiently downregulates the protein (Fig 4A and (34)). Using the RBD precipitation assay, we compared the depolarization-induced Rho activation in control cells (transfected with a non-related siRNA) and in GEF-H1 downregulated cells. As shown in Fig 4A, in control siRNA transfected cells K^+-medium caused well-detectable Rho activation. In contrast, depolarization failed to activate Rho in cells lacking GEF-H1.

We have demonstrated in our previous work (57) that depolarization induces Rho and Rho kinase-dependent MLC phosphorylation. Therefore, we next investigated the effect of GEF-H1 downregulation on the depolarization-induced MLC phosphorylation. Differentially phosphorylated MLC forms were detected using urea-glycerol PAGE. LLC-PK1 cells contain two isoforms of MLC, which exist in non-phosphorylated, mono-phosphorylated (Ser 19) and di-phosphorylated (Ser19 and Thr18) forms (Fig 4B), as shown in our earlier papers (16, 57). Depolarization, as expected, induced an increase in di-phospho-MLC. Importantly, this effect was eliminated by the GEF-H1 siRNA (Fig 4B), verifying the critical role of this exchange factor in the depolarization-induced myosin activation.

To show that the upstream signaling is intact in cells devoid of GEF-H1, we followed ERK phosphorylation in cells treated with NR or GEF-H1 siRNA. As shown on Fig 4C, GEF-H1 downregulation had no effect on depolarization-induced ERK activation. The increase in pERK levels was identical in cells treated with control or GEF-H1 specific siRNA (Fig 4C). Therefore, the observed inhibitory effects of GEF-H1 downregulation are not due to unresponsiveness of the cells or an inhibition of upstream signaling.

Inhibition of the Na^+/K^+ ATPase induces ERK phosphorylation partly through depolarization

The function of the Na^+/K^+ ATPase is indispensable for establishing and maintaining the resting membrane potential, because the pump maintains the transmembrane Na^+ and K^+ concentration gradients. In addition, its electrogenic action directly contributes to the resting potential. Interestingly, ouabain, an inhibitor of the Na^+ pump was shown to induce ERK activation in various cells including proximal tubule epithelia (19, 37, 44). Having demonstrated that depolarization activates ERK, we wondered, whether depolarization might contribute to the effect of ouabain on ERK. We first established the kinetics of ouabain-induced ERK activation in LLC-PK1 cells. As shown on Fig 5A, exposure of LLC-PK1 cells to 1 mM ouabain caused well detectable ERK activation after 5 minutes. Moreover, removal

of extracellular K^+, which blocks the pump, also elicited ERK phosphorylation, suggesting that inhibition of the Na^+ pump is indeed key for the effect (Fig 5A right blot). Next we wished to test whether depolarization contributes to the ERK-activating effect of ouabain. To achieve this, we clamped the membrane potential using the K^+-ionophore valinomycin. As expected, in the presence of 10 mM extracellular K^+, valinomycin treatment caused no major change in the basal pERK levels (Fig 5B). Importantly, when ouabain was added in the presence of valinomycin, ERK phosphorylation was reduced (by ≈50%, $p \leq 0.001$). To rule out any non-specific inhibitory effects of valinomycin on the ERK pathway itself, we also tested its effect on the Epidermal Growth Factor (EGF)-induced ERK activation (Fig 5C). EGF caused identical elevation in the levels of pERK in the absence or presence of valinomycin. These data therefore suggest that depolarization contributes to the ouabain-induced ERK activation.

Ouabain has recently emerged as a signal initiator that binds to the pump and exerts effects in concentrations that are below the pump-inhibiting concentrations (reviewed in (67)). While ouabain in such low concentration can initiate signaling, it does not induce depolarization (19, 42). As shown on Fig 5D, 1 and 10 nM ouabain was indeed able to increase levels of pERK. Moreover, when ERK phosphorylation was induced by 10 nM ouabain, valinomycin did not inhibit, but slightly enhanced the response (Fig 5E). This finding is in complete agreement with the fact that ouabain at this low concentration does not cause depolarization. Taken together, these data suggest that higher ouabain concentrations stimulate ERK partly through depolarization-independent and partly through depolarization-dependent mechanisms.

Inhibition of the Na^+/K^+ ATPase induces GEF-H1-dependent Rho activation

While ouabain was shown to affect the cytoskeleton (18, 33), its effect on Rho is not known. As ouabain potently activates ERK, it was conceivable that it might also activate Rho. Indeed, as shown on Fig 6, ouabain treatment causes substantial Rho activation. Importantly, this effect was prevented by downregulation of GEF-H1.

Taken together, these data strongly suggest that inhibition of the Na^+ pump by ouabain, similar to other depolarizing effects, can activate the ERK/GEF-H1/Rho pathway.

Depolarization elevates paracellular permeability in a phospho-myosin-dependent manner

Myosin phosphorylation is a central regulator of the intercellular junctions that has been shown to mediate elevation in paracellular permeability by a number of chemical and physical factors (32, 36, 45, 54). In our previous work we have raised the possibility that depolarization could serve as a coupling factor mediating the effects of Na^+-cotransporters on paracellular permeability (36, 57). To assess whether high K^+ can indeed lead to enhanced paracellular permeability, we measured the transepithelial transport of small molecular weight (4 kDa) fluorescent dextran, as in our earlier study (34). Confluent LLC-PK_1 or MDCK layers grown on semipermeable filters were exposed to fluorescent dextran given from the apical side and the transport of dextran through the epithelial layer was assessed by sampling the bottom compartment after 3 hours. We have shown previously (34) that in Na^+-medium both LLC-PK1 and MDCK cells formed tight monolayers, and allowed

only a small amount of dextran to permeate through the paracellular pathway throughout a 3-hour period. When dextran permeability was followed in the K^+-medium, fluorescence increased much faster: a 2.9-fold and 5-fold increase was observed for LLC-PK1 and MDCK cells, respectively (Fig 7A and C). Exposure of LLC-PK1 cells to alanine also enhanced paracellular permeability, although to a smaller extent (Fig 7B).

To test the role of MLC phosphorylation in mediating this permeability increase, we used blebbistatin, a myosin ATPase inhibitor (41, 56). As shown on Fig 7C, blebbistatin inhibited the depolarization-induced rise in permeability in a concentration-dependent manner.

To substantiate these results using a non-pharmacological approach, we took advantage of an LLC-PK1 cell line expressing a mutant, non-phosphorylatable MLC in which threonine 18 and serine 19 were changed to alanines (AA-MLC) (34). We have previously shown that this mutant does not disrupt the basal actin cytoskeleton, but prevents MLC phosphorylation induced by hyperosmolarity, depolarization and TNF-α (16, 34). As expected, in control cells expressing the empty vector, K^+-medium caused an increase in permeability (Fig 7D). In contrast, the permeability of AA-MLC expressing cells was unaltered by the K^+-medium (Fig 7D). This however was not due to a general unresponsiveness of the cells to depolarization, as ERK phosphorylation induced by the K^+-medium was indistinguishable in control and AA-MLC expressing cells (Fig 7E). Taken together, these data suggest that MLC phosphorylation is indispensable for the depolarization-induced permeability elevation.

DISCUSSION

The resting membrane potential in epithelia contributes to the maintenance of cellular ion concentrations and provides driving force for ion transport. This function is indispensable for absorption and secretion taking place through epithelial layers. In the past years, however, it has become clear that depolarization of the plasma membrane alters cell morphology and initiates signaling as well. In epithelia, depolarization induces F-actin assembly (12, 14) and myosin phosphorylation (57). In search for the mechanism mediating these effects, we have shown that depolarization activates the small GTPase Rho in tubular cells (57). The aim of the present study was to gain insight into the mechanism of Rho activation. Our findings show that depolarization activates ERK which in turn mediates activation of the Rho exchange factor GEF-H1, leading to Rho activation.

In neuronal cells depolarization-induced ERK activation has been associated with proliferation and survival (9, 38) and activity-dependent dendrite formation (64). Here we provide evidence for the first time that depolarization also activates ERK in tubular epithelia. Interestingly, in neurons, depolarization-provoked ERK activation depends on a rise in intracellular Ca^{2+} (4, 21, 53). As tubular cells show no changes in intracellular Ca^{2+} upon depolarization (57), the mechanisms for ERK activation likely differs from that observed in neurons. Indeed, the depolarization-induced ERK activation was unaltered when LLC-PK1 cells were loaded with the Ca^{2+} chelator BAPTA, verifying the Ca^{2+} independence of the effect.

We also demonstrate that MEK, the enzyme directly upstream of ERK is activated by depolarization. Two Ras family small GTPases have been implicated in activation of the canonical Raf/MEK/ERK cascade: Rap1 and Ras (28, 49). We show that depolarization activates Ras in epithelial cells, and Ras is necessary for ERK activation. The question of how Ras is activated by depolarization however remains to be answered. One possible scenario is that depolarization might stimulate growth factor receptors, leading to activation of Ras. Indeed, such growth factor receptor transactivation has been described for other physical factors, including UV light and hyperosmolarity (30), as well as for the Na^+-pump inhibitor ouabain (67, 69). In neurons depolarization-induced ERK activation was found to be PKA-dependent (4, 46, 48). The existence of similar mechanisms and the possible role for PKA in tubular cells remains to be investigated. An alternative but non-exclusive mechanism may implicate the direct potential sensitivity of Ras (68). Specifically K-Ras contains a polybasic domain, which is responsible for the surface charge-regulated membrane localization of this GTPase. It remains to be determined whether changes in the transmembrane potential might (indirectly) also affect the distribution/activation of Ras.

One of the key findings of this study is the identification of GEF-H1 as the exchange factor mediating depolarization-induced Rho activation. GEF-H1, a Rho specific GEF, binds to the microtubules and cell junctions (7). Our finding that the depolarization-induced GEF-H1 and Rho activation are prevented by MEK inhibition places ERK upstream of GEF-H1 and Rho activation. Indeed, ERK has been shown to associate with and phosphorylate GEF-H1, resulting in enhanced Rho GEF activity (23). Interestingly, we have previously found that a similar mechanism is responsible for TNF-α-induced Rho activation (34). The crosstalk between ERK and GEF-H1 therefore seems to be a central and general mechanism for modulating Rho activity and the cytoskeleton by various stimuli in the tubular epithelium. Moreover, as Rho is also involved in the regulation of gene expression and cell cycle (65), some of the proliferative effects of ERK might be due to its impact on Rho. In this respect it will be interesting to see whether GEF-H1 and Rho activation contribute to the depolarization-induced proliferative effects in neurons.

Our studies implicate GEF-H1 as a membrane potential-sensitive GEF in epithelial cells. Interestingly, GEF-H1 and its mouse homologue, Lfc are highly expressed in the brain as well, and are thought to have a role in the development of spine density and neuronal plasticity (35, 51). Moreover, KCl-induced depolarization results in the translocation of GEF-H1 to the dendritic spines (51). In addition, GEF-H1 has recently been identified as a component of the AMPA receptor complex (35), and its activity was shown to negatively regulate spine density and length through RhoA. These data suggest that depolarization of neurons might affect neuronal plasticity through GEF-H1. This intriguing possibility remains to be investigated.

Besides its role as a regulator of Na^+ and K^+ homeostasis and membrane potential, the Na^+/K^+ pump has also emerged as a signal initiator (reviewed in (67, 69). Upon ouabain biding, the pump interacts with various membrane proteins, which leads to activation of Src, the EGF receptor and the ERK pathway. However, the classic effect of ouabain (when used in the usual 0.5–1 mM concentration range) is the inhibition of the Na^+ pump. This involves the cessation of its electrogenic activity thereby causing depolarization. Therefore we

wondered whether this depolarizing effect might contribute to ERK activation. To assess this, we clamped the membrane potential using valinomycin during ouabain treatment. This manoeuvre partially prevented ERK activation by ouabain, suggesting that depolarization is indeed a contributing factor. Our finding that inhibition of the pump by K^+ removal also results in ERK activation further argues against the notion that the effect is exclusively due to ouabain binding. A significant portion of the effect of ouabain, however, seems to be independent of the potential changes. Indeed, as shown by others (19, 42), low concentrations of ouabain (1 or 10 nM), which do not cause significant depolarization also induced ERK activation. This effect however was not prevented by valinomycin. Moreover, in agreement with other studies (25, 66, 67) we have found that ouabain-induced ERK activation requires Src family kinases, as this effect was eliminated by the Src inhibitor PP2 (not shown). These data substantiate earlier findings that ouabain can stimulate signalling independent of its pump-inhibiting effect and call attention to the fact that ouabain affects ERK both by potential-dependent and independent pathways.

Another novel finding of this study is that ouabain induces Rho activation in tubular cells, and this effect is mediated by GEF-H1. These findings are in agreement with data from renal arterial smooth muscle cells, where ouabain was shown to induce ROK-dependent myosin phosphorylation and contraction (2). Interestingly, in HeLa cells ouabain was shown to downregulate the Rho kinase/LIM kinase/cofilin pathway through the MEK/ERK pathway (33). Strangely, ROK inactivation was not accompanied by a decrease in Rho activity in these studies. While the reason for the apparent discrepancies between the observations made in HeLa and LLC-PK1 cells is not clear, they might represent cell-type specific differences.

Finally, we considered the effects of depolarization on the epithelial intercellular junctions. Interestingly, apical electrogenic transporters, which can alter the membrane potential, have been shown to enhance paracellular transport. This phenomenon, as described in the intestine, likely increases the efficiency of solute absorption through the epithelial layer (47, 61, 62). Importantly, the increase in the permeability of the paracellular pathway induced by apical Na^+-glucose cotransport was shown to be mediated by myosin phosphorylation(61). Further, our earlier studies have shown that activation of the Na^+-alanine transporter induces depolarization as well as myosin phosphorylation in tubular cells (57). Based on these studies, we hypothesized that depolarization might serve as the signal that mediates coupling between apical and paracellular transport (36). The results presented here are in line with this idea. We have found that depolarization indeed enhances paracellular permeability through myosin phosphorylation. Interestingly, although the coupling requires MLC phosphorylation in both intestinal and tubular cells, our current and previous studies reveal that the mechanisms leading to MLC phosphorylation differ in the two cell types. In intestinal epithelium, the apical cotransporters affect MLCK, which is activated through a change in the intracellular pH caused by the combined effects of the Na^+ glucose cotransporter and the Na/H exchanger (reviewed in (36, 61)). In contrast, in tubular cells apical Na^+-alanine cotransport induces MLC phosphorylation through depolarization, activating Rho and ROK (57). The current work shows that this occurs through ERK-dependent GEF-H1 activation. Importantly, GEF-H1 can indeed regulate transepithelial and endothelial permeability. GEF-H1 overexpression in MDCK cells resulted in increased

paracellular permeability (6), and it was found to mediate thrombin-induced permeability increase in lung endothelial cells (8). Unfortunately we were not able to test the effect of the GEF-H1 siRNA on transepithelial permeability in this study, as under our conditions the tubular cells failed to form a tight monolayer in the absence of GEF-H1 (34).

Taken together, we propose that the following sequence of events is responsible for the coordination of transport through the apical electrogenic transporters and the paracellular pathway: the electrogenic transporters cause plasma membrane depolarization, which in turn activates the ERK/GEF-H1/Rho/Rho kinase pathway, leading to enhanced MLC phosphorylation and increased paracellular transport.

While numerous studies have revealed that the junctional acto-myosin complex has a key role in regulating TJ permeability (reviewed in (32, 36, 59, 60)), the underlying mechanism remains elusive. Myosin II in epithelial cells is enriched in the perijunctional actin belt (32). Junctional transmembrane proteins, including occludin and claudins are directly or indirectly linked to the junctional actin (27), and myosin has been shown to directly bind to the TJ through the adapter protein cingulin (15). This direct physical contact with the acto-myosin belt raises the possibility that increased myosin-mediated contractility may exert a mechanical effect, physically pulling the junctions apart. In addition, dynamic junction remodeling was also shown to involve altered expression, phosphorylation, endocytosis and exocytosis of junctional components (11, 27). These mechanisms might also depend on myosin. Interestingly, various stimuli, including Ca^{2+}-removal (52), interferon-γ (63) and house dust mite (29) induce MLC-dependent endocytosis of adherens junction proteins. As occludin can also undergo endocytosis (58), our ongoing studies are aimed at testing whether depolarization induces MLC-dependent changes in occludin or claudin traffic.

In summary, we have shown that depolarization-induced activation of the Rho pathway is mediated by ERK and GEF-H1. Depolarization also enhances the paracellular permeability in a phospho-myosin-dependent way. These mechanisms likely play an important role in the regulation of tight junctions and the coordination between transepithelial and paracellular transport.

Acknowledgments

The authors would like to thank Dr. Andras Masszi for expert advice and critical reading of the manuscript. This work was supported by grants from the Natural Sciences and Engineering Research Council of Canada (NSERC, grant nr: 480619) and the Banting Foundation to KS and by the Kidney Foundation of Canada to AK and KS. KS is a recipient of a KRESCENT New Investigator Award (a joint award of the Kidney Foundation of Canada, Canadian Nephrology Society and Canadian Institute of Health Research).

References

1. Aittaleb M, Boguth CA, Tesmer JJ. Structure and function of heterotrimeric G protein-regulated Rho guanine nucleotide exchange factors. Mol Pharmacol. 2010; 77:111–125. [PubMed: 19880753]
2. Ark M, Kubat H, Beydagi H, Ergenoglu T, Songu-Mize E. Involvement of rho kinase in the ouabain-induced contractions of the rat renal arteries. Biochem Biophys Res Commun. 2006; 340:417–421. [PubMed: 16375858]
3. Arya R, Mallik M, Lakhotia SC. Heat shock genes - integrating cell survival and death. J Biosci. 2007; 32:595–610. [PubMed: 17536179]

4. Baldassa S, Zippel R, Sturani E. Depolarization-induced signaling to Ras, Rap1 and MAPKs in cortical neurons. Brain Res Mol Brain Res. 2003; 119:111–122. [PubMed: 14597235]
5. Balestrino M. Pathophysiology of anoxic depolarization: new findings and a working hypothesis. J Neurosci Methods. 1995; 59:99–103. [PubMed: 7475257]
6. Benais-Pont G, Punn A, Flores-Maldonado C, Eckert J, Raposo G, Fleming TP, Cereijido M, Balda MS, Matter K. Identification of a tight junction-associated guanine nucleotide exchange factor that activates Rho and regulates paracellular permeability. J Cell Biol. 2003; 160:729–740. [PubMed: 12604587]
7. Birkenfeld J, Nalbant P, Yoon SH, Bokoch GM. Cellular functions of GEF-H1, a microtubule-regulated Rho-GEF: is altered GEF-H1 activity a crucial determinant of disease pathogenesis? Trends Cell Biol. 2008; 18:210–219. [PubMed: 18394899]
8. Birukova AA, Adyshev D, Gorshkov B, Bokoch GM, Birukov KG, Verin AD. GEF-H1 is involved in agonist-induced human pulmonary endothelial barrier dysfunction. Am J Physiol Lung Cell Mol Physiol. 2006; 290:L540–548. [PubMed: 16257999]
9. Borodinsky LN, Fiszman ML. Extracellular potassium concentration regulates proliferation of immature cerebellar granule cells. Brain Res Dev Brain Res. 1998; 107:43–48. [PubMed: 9602050]
10. Brzezinska AK, Lohr N, Chilian WM. Electrophysiological effects of O2*-on the plasma membrane in vascular endothelial cells. Am J Physiol Heart Circ Physiol. 2005; 289:H2379–2386. [PubMed: 15964927]
11. Capaldo CT, Nusrat A. Cytokine regulation of tight junctions. Biochim Biophys Acta. 2009; 1788:864–871. [PubMed: 18952050]
12. Chifflet S, Correa V, Nin V, Justet C, Hernandez JA. Effect of membrane potential depolarization on the organization of the actin cytoskeleton of eye epithelia. The role of adherens junctions. Exp Eye Res. 2004; 79:769–777. [PubMed: 15642314]
13. Chifflet S, Hernandez JA, Grasso S. A possible role for membrane depolarization in epithelial wound healing. Am J Physiol Cell Physiol. 2005; 288:C1420–1430. [PubMed: 15897322]
14. Chifflet S, Hernandez JA, Grasso S, Cirillo A. Nonspecific depolarization of the plasma membrane potential induces cytoskeletal modifications of bovine corneal endothelial cells in culture. Exp Cell Res. 2003; 282:1–13. [PubMed: 12490189]
15. Cordenonsi M, D'Atri F, Hammar E, Parry DA, Kendrick-Jones J, Shore D, Citi S. Cingulin contains globular and coiled-coil domains and interacts with ZO-1, ZO-2, ZO-3, and myosin. J Cell Biol. 1999; 147:1569–1582. [PubMed: 10613913]
16. Di Ciano-Oliveira C, Lodyga M, Fan L, Szaszi K, Hosoya H, Rotstein OD, Kapus A. Is myosin light-chain phosphorylation a regulatory signal for the osmotic activation of the Na+-K+-2Cl-cotransporter? Am J Physiol Cell Physiol. 2005; 289:C68–81. [PubMed: 15728707]
17. Di Ciano-Oliveira C, Sirokmany G, Szaszi K, Arthur WT, Masszi A, Peterson M, Rotstein OD, Kapus A. Hyperosmotic stress activates Rho: differential involvement in Rho kinase-dependent MLC phosphorylation and NKCC activation. Am J Physiol Cell Physiol. 2003; 285:C555–566. [PubMed: 12748065]
18. Dismuke WM, Mbadugha CC, Faison D, Ellis DZ. Ouabain-induced changes in aqueous humour outflow facility and trabecular meshwork cytoskeleton. Br J Ophthalmol. 2009; 93:104–109. [PubMed: 18971239]
19. Dmitrieva RI, Doris PA. Ouabain is a potent promoter of growth and activator of ERK1/2 in ouabain-resistant rat renal epithelial cells. J Biol Chem. 2003; 278:28160–28166. [PubMed: 12736249]
20. Duquesnes N, Vincent F, Morel E, Lezoualc'h F, Crozatier B. The EGF receptor activates ERK but not JNK Ras-dependently in basal conditions but ERK and JNK activation pathways are predominantly Ras-independent during cardiomyocyte stretch. Int J Biochem Cell Biol. 2009; 41:1173–1181. [PubMed: 19015044]
21. Egea J, Espinet C, Comella JX. Calmodulin modulates mitogen-activated protein kinase activation in response to membrane depolarization in PC12 cells. J Neurochem. 1998; 70:2554–2564. [PubMed: 9603222]

22. Enslen H, Tokumitsu H, Stork PJ, Davis RJ, Soderling TR. Regulation of mitogen-activated protein kinases by a calcium/calmodulin-dependent protein kinase cascade. Proc Natl Acad Sci U S A. 1996; 93:10803–10808. [PubMed: 8855261]
23. Fujishiro SH, Tanimura S, Mure S, Kashimoto Y, Watanabe K, Kohno M. ERK1/2 phosphorylate GEF-H1 to enhance its guanine nucleotide exchange activity toward RhoA. Biochem Biophys Res Commun. 2008; 368:162–167. [PubMed: 18211802]
24. Garcia-Mata R, Wennerberg K, Arthur WT, Noren NK, Ellerbroek SM, Burridge K. Analysis of activated GAPs and GEFs in cell lysates. Methods Enzymol. 2006; 406:425–437. [PubMed: 16472675]
25. Haas M, Wang H, Tian J, Xie Z. Src-mediated inter-receptor cross-talk between the Na+/K+-ATPase and the epidermal growth factor receptor relays the signal from ouabain to mitogen-activated protein kinases. J Biol Chem. 2002; 277:18694–18702. [PubMed: 11907028]
26. Haddad GG, Donnelly DF. O2 deprivation induces a major depolarization in brain stem neurons in the adult but not in the neonatal rat. J Physiol. 1990; 429:411–428. [PubMed: 2126043]
27. Hartsock A, Nelson WJ. Adherens and tight junctions: Structure, function and connections to the actin cytoskeleton. Biochim Biophys Acta. 2007
28. Hattori M, Minato N. Rap1 GTPase: functions, regulation, and malignancy. J Biochem. 2003; 134:479–484. [PubMed: 14607972]
29. Heijink IH, Postma DS, Noordhoek JA, Broekema M, Kapus A. House dust mite-promoted epithelial-to-mesenchymal transition in human bronchial epithelium. Am J Respir Cell Mol Biol. 42:69–79.
30. Higashiyama S, Iwabuki H, Morimoto C, Hieda M, Inoue H, Matsushita N. Membrane-anchored growth factors, the epidermal growth factor family: beyond receptor ligands. Cancer Sci. 2008; 99:214–220. [PubMed: 18271917]
31. Hoyer J, Gogelein H. Sodium-alanine cotransport in renal proximal tubule cells investigated by whole-cell current recording. J Gen Physiol. 1991; 97:1073–1094. [PubMed: 1650810]
32. Ivanov AI. Actin motors that drive formation and disassembly of epithelial apical junctions. Front Biosci. 2008; 13:6662–6681. [PubMed: 18508686]
33. Jung J, Kim M, Choi S, Kim MJ, Suh JK, Choi EC, Lee K. Molecular mechanism of cofilin dephosphorylation by ouabain. Cell Signal. 2006; 18:2033–2040. [PubMed: 16713181]
34. Kakiashvili E, Speight P, Waheed F, Seth R, Lodyga M, Tanimura S, Kohno M, Rotstein OD, Kapus A, Szaszi K. GEF-H1 Mediates Tumor Necrosis Factor-{alpha}-induced Rho Activation and Myosin Phosphorylation: role in the regulation of tubular paracellular permeability. J Biol Chem. 2009; 284:11454–11466. [PubMed: 19261619]
35. Kang MG, Guo Y, Huganir RL. AMPA receptor and GEF-H1/Lfc complex regulates dendritic spine development through RhoA signaling cascade. Proc Natl Acad Sci U S A. 2009; 106:3549–3554. [PubMed: 19208802]
36. Kapus A, Szaszi K. Coupling between apical and paracellular transport processes. Biochem Cell Biol. 2006; 84:870–880. [PubMed: 17215874]
37. Khundmiri SJ, Amin V, Henson J, Lewis J, Ameen M, Rane MJ, Delamere NA. Ouabain stimulates protein kinase B (Akt) phosphorylation in opossum kidney proximal tubule cells through an ERK-dependent pathway. Am J Physiol Cell Physiol. 2007; 293:C1171–1180. [PubMed: 17634416]
38. Kim TW, Lee CH, Choi CY, Kwon NS, Baek KJ, Kim YG, Yun HY. Nitric oxide mediates membrane depolarization-promoted survival of rat neuronal PC12 cells. Neurosci Lett. 2003; 344:209–211. [PubMed: 12812842]
39. Koivusalo M, Kapus A, Grinstein S. Sensors, transducers, and effectors that regulate cell size and shape. J Biol Chem. 2009; 284:6595–6599. [PubMed: 19004817]
40. Krendel M, Zenke FT, Bokoch GM. Nucleotide exchange factor GEF-H1 mediates cross-talk between microtubules and the actin cytoskeleton. Nat Cell Biol. 2002; 4:294–301. [PubMed: 11912491]
41. Limouze J, Straight AF, Mitchison T, Sellers JR. Specificity of blebbistatin, an inhibitor of myosin II. J Muscle Res Cell Motil. 2004; 25:337–341. [PubMed: 15548862]

42. Liu J, Tian J, Haas M, Shapiro JI, Askari A, Xie Z. Ouabain interaction with cardiac Na+/K+-ATPase initiates signal cascades independent of changes in intracellular Na+ and Ca2+ concentrations. J Biol Chem. 2000; 275:27838–27844. [PubMed: 10874029]
43. Masszi A, Speight P, Charbonney E, Lodyga M, Nakano H, Szaszi K, Kapus A. Fate-determining mechanisms in epithelial-myofibroblast transition: major inhibitory role for Smad3. J Cell Biol. 2010; 188:383–399. [PubMed: 20123992]
44. Nguyen AN, Wallace DP, Blanco G. Ouabain binds with high affinity to the Na,K-ATPase in human polycystic kidney cells and induces extracellular signal-regulated kinase activation and cell proliferation. J Am Soc Nephrol. 2007; 18:46–57. [PubMed: 17151336]
45. Nusrat A, Turner JR, Madara JL. Molecular physiology and pathophysiology of tight junctions. IV. Regulation of tight junctions by extracellular stimuli: nutrients, cytokines, and immune cells. Am J Physiol Gastrointest Liver Physiol. 2000; 279:G851–857. [PubMed: 11052980]
46. Obara Y, Horgan AM, Stork PJ. The requirement of Ras and Rap1 for the activation of ERKs by cAMP, PACAP, and KCl in cerebellar granule cells. J Neurochem. 2007; 101:470–482. [PubMed: 17254020]
47. Pappenheimer JR. On the coupling of membrane digestion with intestinal absorption of sugars and amino acids. Am J Physiol. 1993; 265:G409–417. [PubMed: 8214061]
48. Park JH, Park JK, Bae KW, Park HT. Protein kinase A activity is required for depolarization-induced proline-rich tyrosine kinase 2 and mitogen-activated protein kinase activation in PC12 cells. Neurosci Lett. 2000; 290:25–28. [PubMed: 10925166]
49. Ramos JW. The regulation of extracellular signal-regulated kinase (ERK) in mammalian cells. Int J Biochem Cell Biol. 2008; 40:2707–2719. [PubMed: 18562239]
50. Rossman KL, Der CJ, Sondek J. GEF means go: turning on RHO GTPases with guanine nucleotide-exchange factors. Nat Rev Mol Cell Biol. 2005; 6:167–180. [PubMed: 15688002]
51. Ryan XP, Alldritt J, Svenningsson P, Allen PB, Wu GY, Nairn AC, Greengard P. The Rho-specific GEF Lfc interacts with neurabin and spinophilin to regulate dendritic spine morphology. Neuron. 2005; 47:85–100. [PubMed: 15996550]
52. Samarin SN, Ivanov AI, Flatau G, Parkos CA, Nusrat A. Rho/ROCK-II Signaling Mediates Disassembly of Epithelial Apical Junctions. Mol Biol Cell. 2007
53. Schmitt JM, Wayman GA, Nozaki N, Soderling TR. Calcium activation of ERK mediated by calmodulin kinase I. J Biol Chem. 2004; 279:24064–24072. [PubMed: 15150258]
54. Shen L, Black ED, Witkowski ED, Lencer WI, Guerriero V, Schneeberger EE, Turner JR. Myosin light chain phosphorylation regulates barrier function by remodeling tight junction structure. J Cell Sci. 2006; 119:2095–2106. [PubMed: 16638813]
55. Sohn HY, Keller M, Gloe T, Morawietz H, Rueckschloss U, Pohl U. The small G-protein Rac mediates depolarization–induced superoxide formation in human endothelial cells. J Biol Chem. 2000; 275:18745–18750. [PubMed: 10764736]
56. Straight AF, Cheung A, Limouze J, Chen I, Westwood NJ, Sellers JR, Mitchison TJ. Dissecting temporal and spatial control of cytokinesis with a myosin II Inhibitor. Science. 2003; 299:1743–1747. [PubMed: 12637748]
57. Szaszi K, Sirokmany G, Di Ciano-Oliveira C, Rotstein OD, Kapus A. Depolarization induces Rho-Rho kinase-mediated myosin light chain phosphorylation in kidney tubular cells. Am J Physiol Cell Physiol. 2005; 289:C673–685. [PubMed: 15857905]
58. Terai T, Nishimura N, Kanda I, Yasui N, Sasaki T. JRAB/MICAL-L2 is a junctional Rab13-binding protein mediating the endocytic recycling of occludin. Mol Biol Cell. 2006; 17:2465–2475. [PubMed: 16525024]
59. Terry S, Nie M, Matter K, Balda MS. Rho signaling and tight junction functions. Physiology (Bethesda). 2010; 25:16–26. [PubMed: 20134025]
60. Turner JR. Molecular basis of epithelial barrier regulation: from basic mechanisms to clinical application. Am J Pathol. 2006; 169:1901–1909. [PubMed: 17148655]
61. Turner JR. Show me the pathway! Regulation of paracellular permeability by Na(+)–glucose cotransport. Adv Drug Deliv Rev. 2000; 41:265–281. [PubMed: 10854686]

62. Turner JR, Madara JL. Physiological regulation of intestinal epithelial tight junctions as a consequence of Na(+)-coupled nutrient transport. Gastroenterology. 1995; 109:1391–1396. [PubMed: 7557112]

63. Utech M, Ivanov AI, Samarin SN, Bruewer M, Turner JR, Mrsny RJ, Parkos CA, Nusrat A. Mechanism of IFN-gamma-induced endocytosis of tight junction proteins: myosin II-dependent vacuolarization of the apical plasma membrane. Mol Biol Cell. 2005; 16:5040–5052. [PubMed: 16055505]

64. Vaillant AR, Zanassi P, Walsh GS, Aumont A, Alonso A, Miller FD. Signaling mechanisms underlying reversible, activity-dependent dendrite formation. Neuron. 2002; 34:985–998. [PubMed: 12086645]

65. Vega FM, Ridley AJ. Rho GTPases in cancer cell biology. FEBS Lett. 2008; 582:2093–2101. [PubMed: 18460342]

66. Wang H, Haas M, Liang M, Cai T, Tian J, Li S, Xie Z. Ouabain assembles signaling cascades through the caveolar Na+/K+-ATPase. J Biol Chem. 2004; 279:17250–17259. [PubMed: 14963033]

67. Xie Z. Molecular mechanisms of Na/K-ATPase-mediated signal transduction. Ann N Y Acad Sci. 2003; 986:497–503. [PubMed: 12763870]

68. Yeung T, Terebiznik M, Yu L, Silvius J, Abidi WM, Philips M, Levine T, Kapus A, Grinstein S. Receptor activation alters inner surface potential during phagocytosis. Science. 2006; 313:347–351. [PubMed: 16857939]

69. Zhang L, Zhang Z, Guo H, Wang Y. Na+/K+-ATPase-mediated signal transduction and Na+/K+-ATPase regulation. Fundam Clin Pharmacol. 2008; 22:615–621. [PubMed: 19049666]

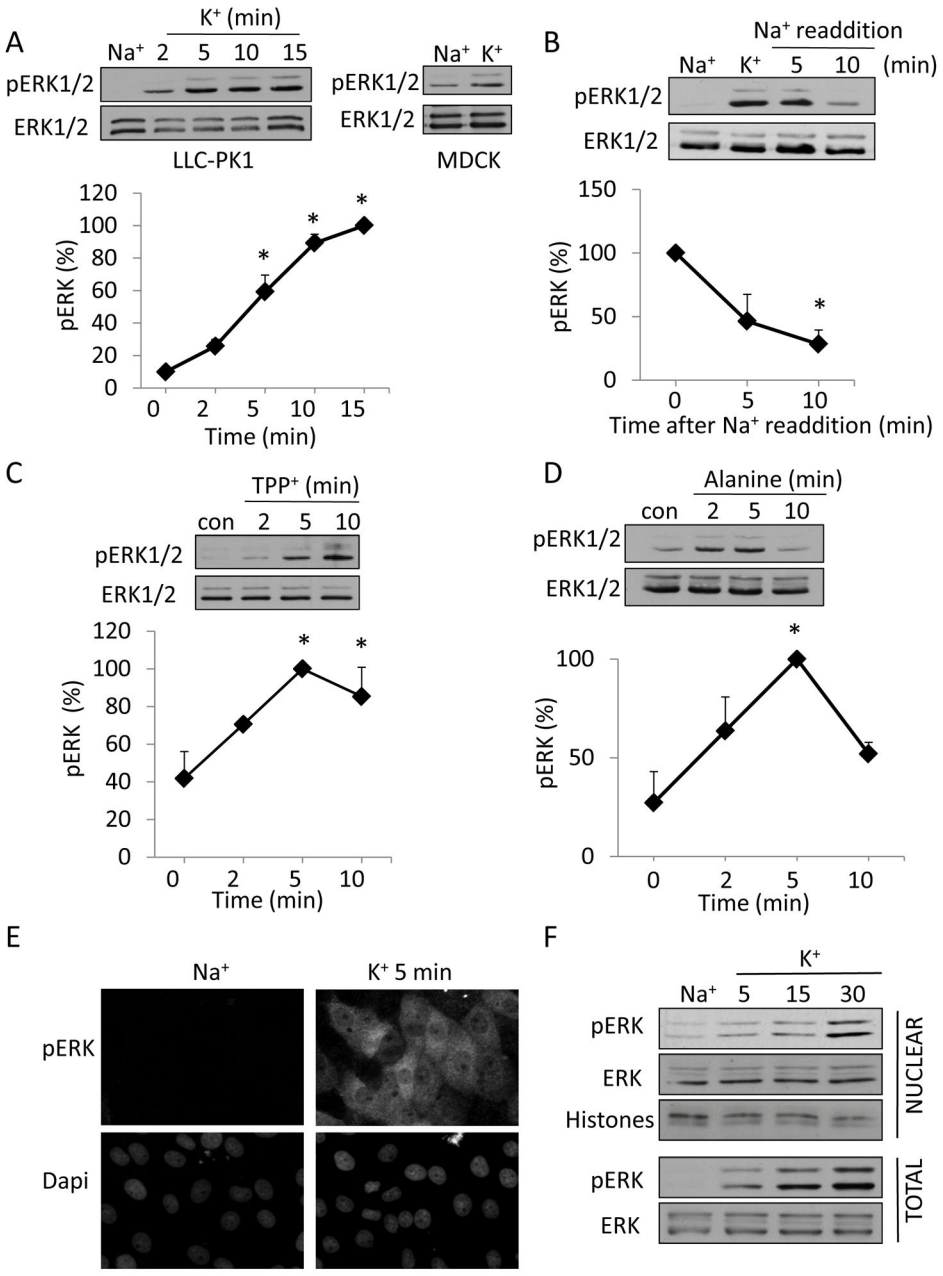

Figure 1. Plasma membrane depolarization induces ERK phosphorylation in epithelial cells

LLC-PK$_1$ (A–D) or MDCK (A) cells grown to confluence were serum-deprived for 3 h and preincubated in Na^+-medium for 15 min. In A and B the cells were treated with Na^+ or K^+ -medium for the indicated times (A) or 10 minutes (B). In B, following the treatment with K^+-medium, the Na^+-medium was added back for the indicated times. In C and D the cells were exposed to 0.5 mM TPP^+ (C) or 20 mM L-Alanine (D). At the end of the treatments, the cells were lysed and total and phosphorylated ERK was detected using Western blotting as described in Materials and Methods. The graphs represent densitometric quantification of pERK Western blots. The values are expressed as the % of the maximal effect, taken as 100%. Data are mean± S.E. (n≥3). Where error bars are not visible, they are smaller than the

symbol. For all panels, * indicates significance vs. 0 min ($p<0.05$). *E,F. Depolarization-induced ERK phosphorylation occurs both in the cytosol and the nucleus. E.* Confluent LLC-PK1 layers, grown on coverslips, were incubated with Na^+ or K^+ -medium for 5 minutes. The cells were fixed and pERK was visualized by immunofluorescence as described in Materials and Methods. Nuclei were visualized using Dapi. *F.* LLC-PK1 cells were grown on 6-cm dishes. Following treatment with Na^+ - or K^+ -medium for the indicated times, the cells were lysed and nuclear fractions were isolated as described in Materials and Methods. The presence of pERK and total ERK in samples containing 10 μg protein was tested using Western blotting. An antibody detecting histones was used to shown equal loading in the nuclear fractions.

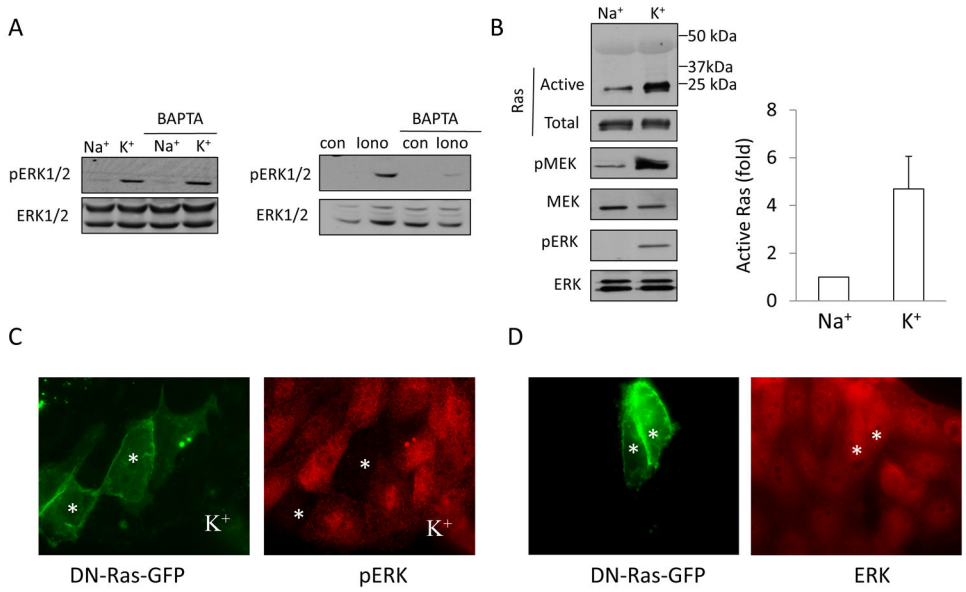

Figure 2.

A. Depolarization-induced ERK activation is Ca^{2+}-independent Cells were preincubated with 30 μM BAPTA-AM in Na^+- medium for 15 minutes prior to exposing them for 5 minutes to Na^+ or K^+-medium (left blots) or 1 μM ionomycin (Iono) (right blots). ERK phosphorylation was detected as in Fig 1. *B. Ras is activated by depolarization.* Cells grown on 10 cm dishes were incubated with Na^+ or K^+-medium for 5 minutes. The cells were lysed and the amount of active Ras was determined using the GST-Ras Binding Domain of c-Raf. Precipitated (active) Ras was detected by Western blotting (top blot). The total cell lysates from the same experiment were also probed with antibodies against Ras, phospho-MEK1/2 (pMEK), total MEK1/2 (MEK), phospho-ERK1/2 (pERK) and total ERK1/2 (ERK). The amount of precipitated (active) Ras was quantified by densitometry and normalized to the amount of total Ras in the cell lysate of the same sample. The results in each experiment were expressed as fold increase compared to the values obtained in control cells. The graph shows mean ± S.E. from n=3 independent experiments. *C. Ras mediates ERK activation.* Cells were transfected with dominant negative K-Ras coupled to GFP (DN-Ras-GFP). Forty-eight hours later the cells were treated with K^+-medium for 30 minutes and pERK was visualized as in A. The images show DN-Ras-GFP and pERK in the same field. The transfected cells are labeled with asterisks. Note, that while pERK is well detectable in non-transfected cells, the presence of DN-Ras prevents the induction of ERK phosphorylation. *D. DN- Ras does not affect total ERK levels.* Cells were transfected with DN-Ras-GFP as in C. Forty-eight hours after transfection the cells were fixed and ERK was detected by immunostaining. The transfected cells are labeled with asterisks.

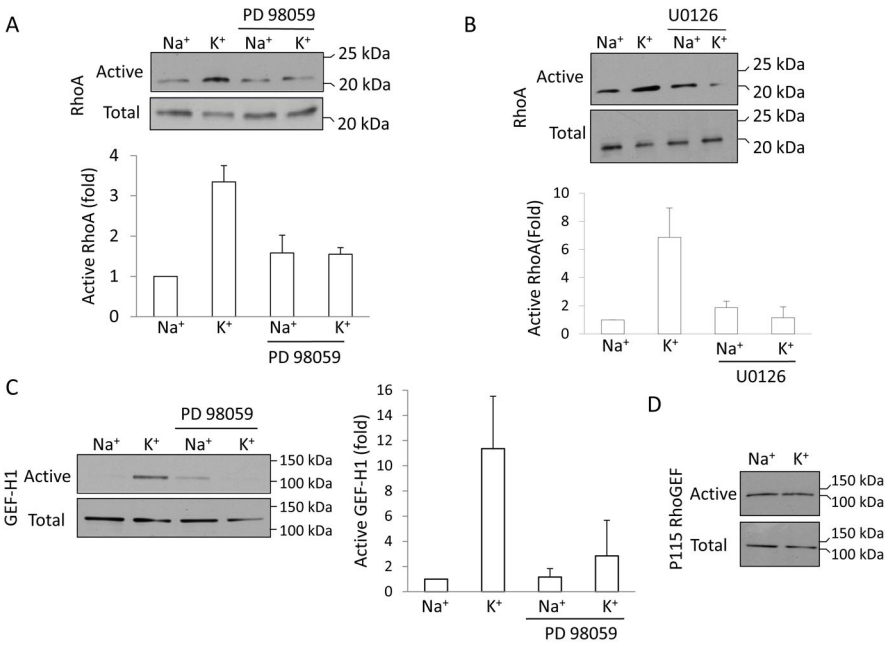

Figure 3. Role of ERK in depolarization-induced activation of GEF-H1 and Rho. A and B

LLC-PK1 cells were treated with 10 μM PD98059 (A) or 10 μM U0126 (B) for 15 min in the Na^+-medium, as indicated, followed by incubation in Na^+or K^+-medium for 5 minutes. The amount of active RhoA was determined using a Rhotekin GST-RBD precipitation assay. RhoA in the precipitates (active RhoA) and total cell lysates (total RhoA) was detected by Western blotting using a RhoA antibody. *C and D.* Active GEF-H1 or p115RhoGEF was precipitated using the GST-RhoG17A. Precipitated (active) and total GEF-H1 (C) or p115RhoGEF (D) was detected by Western blot. The Rho and GEF-H1 blots were quantified by densitometry. The amount of active Rho or GEF-H1 in each sample was normalized to the amount of total RhoA or GEF-H1 in the corresponding cell lysates. The results in each experiment were expressed as fold increase compared to the values obtained in control cells. The graphs show mean ± S.E. from n=3 independent experiments.

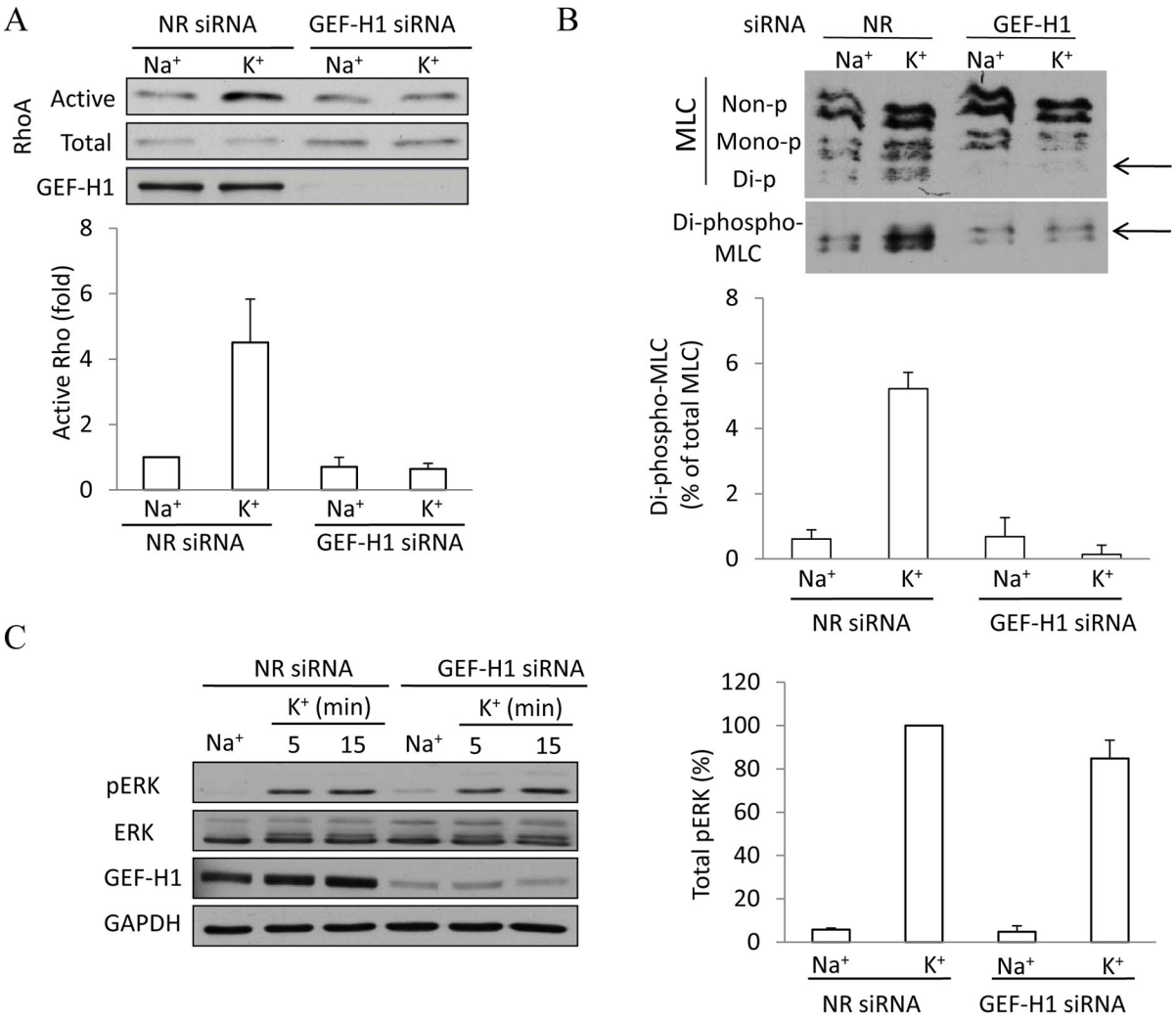

Figure 4. GEF-H1 downregulation prevents depolarization-induced activation of the Rho pathway

LLC-PK$_1$ cells were transfected with non-related (NR) siRNA or an siRNA designed against porcine GEF-H1. Forty-eight hours after transfection cells were treated with Na^+ or K^+ -medium for 5 minutes. *A.* Rho activation was measured and quantified as in Figure 3. GEF-H1 was also detected in the total cell lysates. The graph shows quantification of Rho activation in n=3 independent experiments (mean ± S.E.). *B.* Myosin light chain phosphorylation was detected by Urea-glycerol PAGE as described in Materials and Methods. The blot was developed with an antibody against total MLC, followed by redeveloping with a di-phospho-MLC antibody. LLC-PK1 cells contain two isoforms of MLC, and each can exist as a non-, mono- or di-phosphorylated form as labeled (57). The arrow points to di-phospho-MLC. The graph summarizes densitometric quantification of the changes in di-phospho-MLC. The amount of di-phospho-MLC was expressed as the percentage of the total MLC of the same sample. The results were then expressed as the fold increase compared to the values obtained in control cells (taken as 1). The data represent mean ± S.E. for n=3 independent experiments. *C. GEF-H1 downregulation does not affect*

depolarization-induced ERK phosphorylation. Cells were transfected with NR or GEF-H1 siRNA as above, treated as indicated and ERK and pERK were detected as in Fig 1. An antibody against GAPDH was used to verify equal protein loading. The blots of total cell lysates were also developed with a GEF-H1 antibody to verify downregulation. The blots were analyzed using densitometry as in Fig 1. The graphs represent n=3 independent experiments.

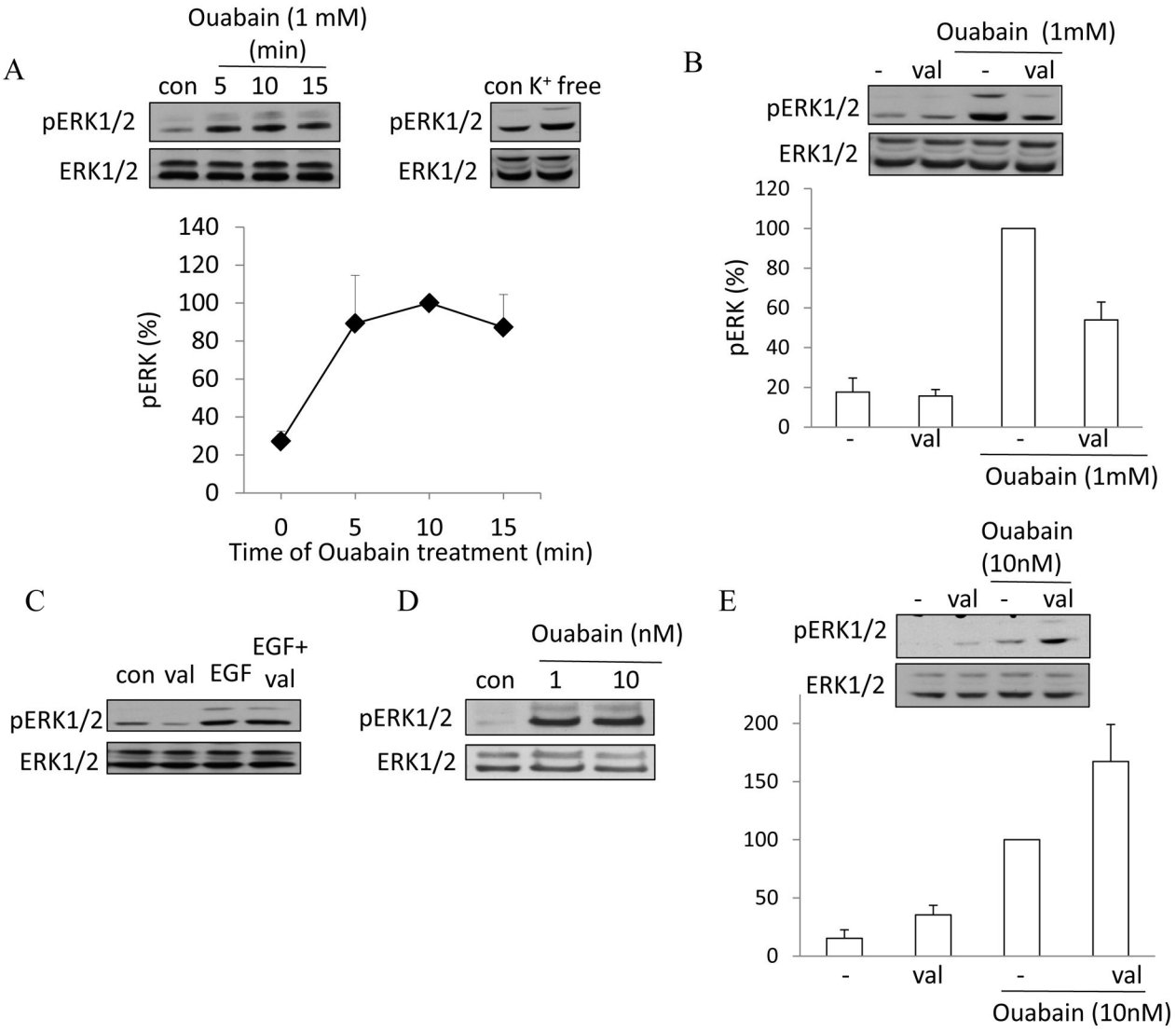

Figure 5. Inhibition of the Na^+/K^+ pump by ouabain induces ERK activation partly through depolarization

LLC-PK_1 cells were subjected to the following treatments: the indicated concentration of ouabain added into the Na^+-medium for the indicated times (A) or 5 minutes (C, D and E); K^+-free medium for 5 minutes (A); 10 μg/ml valinomycin with or without ouabain (B and E) or 10 ng/ml EGF for 5 minutes (C). Where valinomycin was used (B, C and E), the Na^+-medium contained 10 mM K^+. ERK phosphorylation was detected and quantified as in Fig 1. All graphs show data from n=3 experiments (mean ± S.E.).

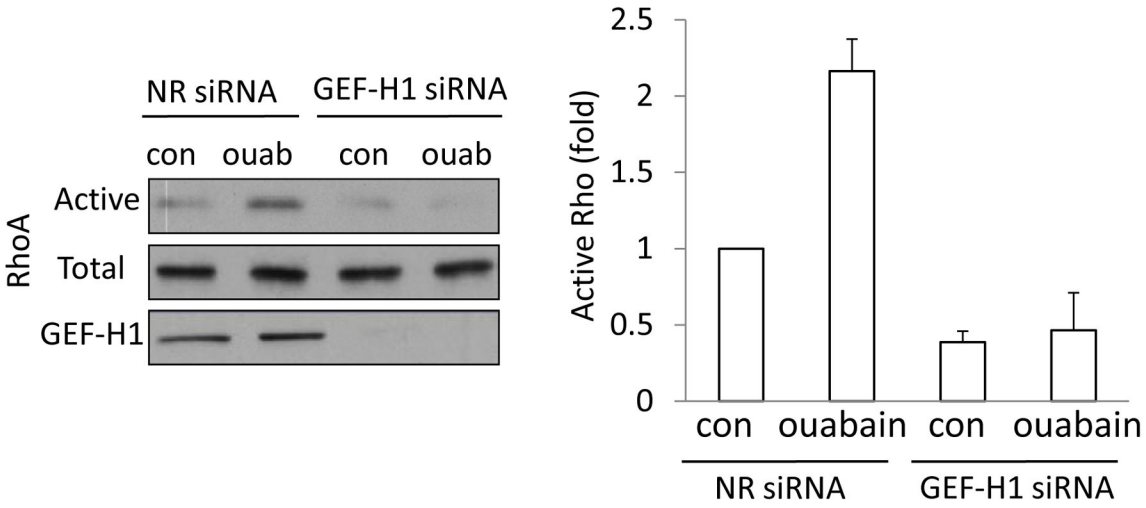

Figure 6. Ouabain activates Rho through GEF-H1

*C*ells were transfected with a non-related (NR) or GEF-H1 specific siRNA. Cells were treated with 1 mM ouabain in Na^+-medium, and Rho activation was determined and quantified as in Figure 3. All graphs show data from n=3 experiments (mean± S.E.).

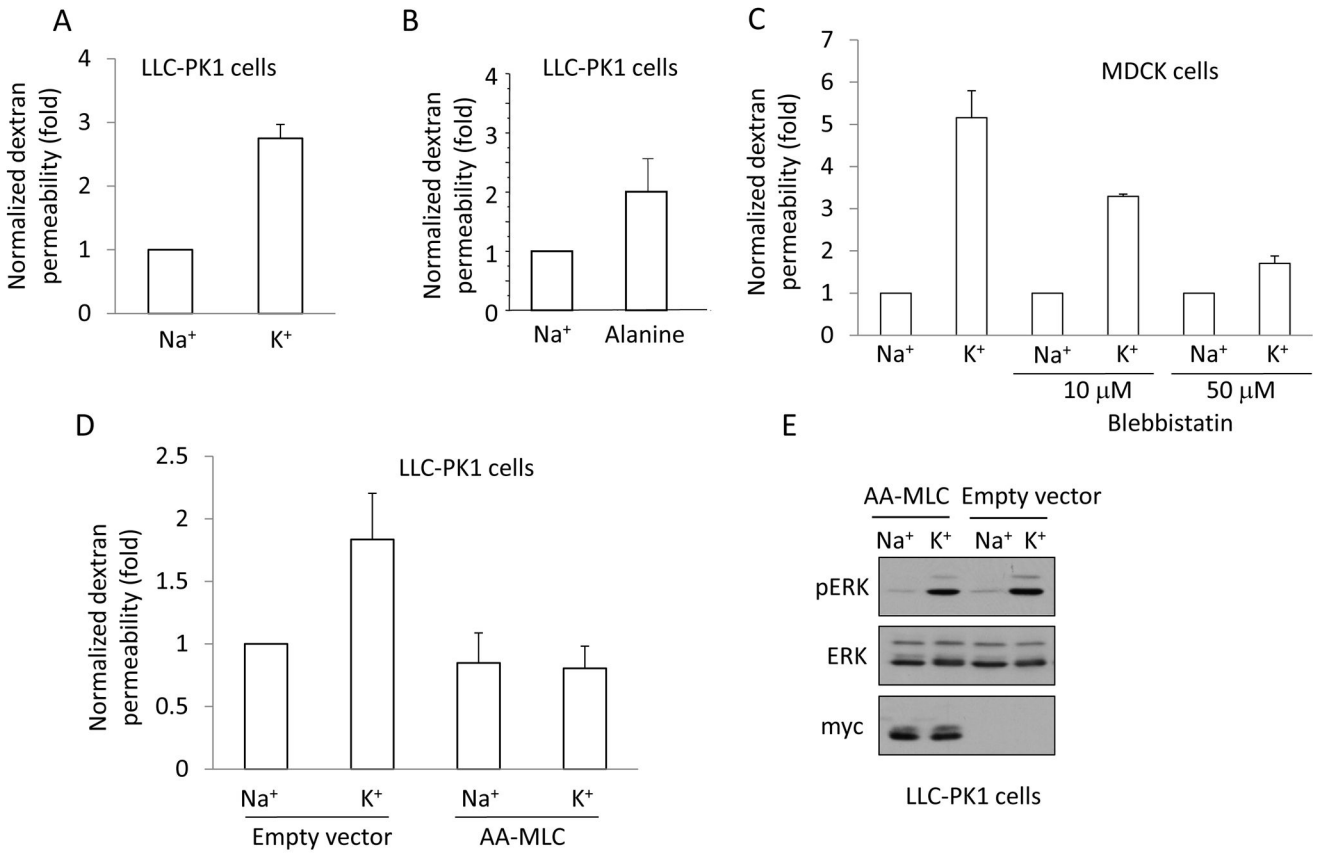

Figure 7. Depolarization elevates paracellular permeability in a pMLC-dependent manner

A–D. LLC-PK$_1$ (A, B) or MDCK (C) or AA-MLC expressing LLC-PK1 cells (D) were grown to confluence on Costar Transwell filters. The medium in both the top and bottom compartments was replaced by Na^+- or K^+-medium and the cells were exposed to 2 mg/ml FITC-labelled dextran (4 kDa) added apically. FITC fluorescence was measured in samples taken from the bottom compartment after 3 hours. The fluorescence values obtained in the triplicate measurements of each experiment were averaged and normalized to the control. The following treatments were used as indicated: Na^+ or K^+ -medium (A,C, D); 20 mM alanine in Na^+-medium (B); 10 or 50 μM blebbistatin pretreatment in Na^+ medium for 30 minutes followed by Na^+- or K^+-medium supplemented with blebbistatin (C). The graphs show the mean ± S.E. from n≥3 experiments. E. *Depolarization induced similar ERK phosphorylation in AA-MLC and control cells.* Empty vector- or AA-MLC-transfected LLC-PK1 cells were treated with Na^+- or K^+-medium for 5 minutes. The cells were lysed and pERK, ERK and myc-tagged AA-MLC were detected by Western blotting.